TECHNICAL PAPER

JOURNAL OF THE SOUTH AFRICAN INSTITUTION OF CIVIL ENGINEERING
ISSN 1021-2019
Vol 59 No 1, March 2017, Pages 28–34, Paper 1385

Numerical modelling of flexible pavement incorporating cross-anisotropic material properties

Part II: Surface rectangular loading

J W Maina, F Kawana, K Matsui

In order to better understand the impact of increased loading on roads, studies on tyre-road interaction have gained prominence in recent years. Tyres form an essential interface between vehicles and road pavement surfaces. These are the only parts of the vehicle that are in contact with the road and transmit the vehicle loading to the road surface. The use of the Cartesian coordinate system is convenient in dealing with a uniform/non-uniform tyre load acting over a rectangular area, but few research reports are available that provide any form of theoretical solutions for pavement responses. This paper presents analytical solutions of responses due to rectangular loading acting on the surface of a multi-layered pavement system. The solutions developed incorporate both isotropic and cross-anisotropic material properties. The method followed is based on classical trigonometric integral and Fourier transformation of Navier's equations. Accuracy and validity of the solutions are verified through comparisons with a proprietary finite element method (FEM) package. For this purpose, a pavement structure composed of five main layers constituted by isotropic and cross-anisotropic (also known as transversely isotropic) material properties is analysed. In order to vary some of the layer properties with depth, the main layers were sub-layered, resulting in a 17-layer pavement system.

PROF JAMES MAINA (Pr Eng, MSAICE, FSAAE) is a professional pavement engineer, full-time professor of civil engineering at the University of Pretoria, and currently on secondment as a technical director of a QA/QC Project for roads in the State of Qatar. He obtained his PhD from Miyazaki University in Japan. His professional activities include QA/QC in road projects, pavement materials, and the development of advanced numerical analysis (modelling) tools for pavement engineering application. He also teaches both under- and post-graduate classes at the University of Pretoria.

Contact details:
Department of Civil Engineering
University of Pretoria
Private Bag X20
Hatfield 0028
South Africa
T: +27 12 420 6608
E: james.maina@up.ac.za

PROF FUTOSHI KAWANA is an associate professor at the Tokyo University of Agriculture in Japan. His specialises in structural mechanics. He received his doctorate in engineering from the Science University of Tokyo in 2004. He is a member of the Japan Society of Civil Engineers, the Pavement Diagnosis Researchers Group (NPO) and the Japanese Society of Irrigation, Drainage and Rural Engineering.

Contact details:
Department of Bioproduction and Environment Engineering
Faculty of Regional Environment Science
Tokyo University of Agriculture
1-1-1 Sakuragaoka
Setagaya-ku
Tokyo, 156-8505
Japan
T: +81 3 5477 2342
E: fk205262@nodai.ac.jp

PROF KUNIHITO MATSUI is emeritus professor of civil and environmental engineering at Tokyo Denki University in Japan. He obtained his PhD from the Department of Mechanics and Hydraulics at the University of Iowa, USA, in 1974. His areas of interest include structural analysis in pavement structures, static and dynamic back-calculation of pavement systems, non-destructive testing, thermal analysis of pavement systems, parameter identification, sensitivity analysis and structural optimisation.

Contact details:
Department of Civil and Environmental Engineering
Tokyo Denki University
Hatoyama
Hiki
Satama, 350-0394
Japan
T: +81 492 96 5703/2549
E: matsui@g.dendai.ac.jp

Keywords: pavement, linear-elastic analysis, transversely isotropic, cross-anisotropy, isotropic, rectangular loading

INTRODUCTION

Motivation for this work is discussed in the companion paper by Maina *et al* (2017), (see pages 22–27 in this edition). Although modern era trucks transport heavier cargo, they are using relatively fewer tyres than their predecessors, and as a result they are purported to be exerting much higher contact stresses on the road surface. A good understanding of tyre-road contact stresses, and the ability to model the macroscopic behaviour of materials when subjected to varying traffic loading and environmental conditions, is therefore important for better road pavement designs and improved pavement performance. Tyres are the only part of the vehicle that are in contact with the road, and transmit the vehicle loading to the road surface through a very small contact area, called the "contact patch" or "tyre footprint". Generally, there are two main types of truck tyres widely used on our roads – the single (or so-called wide-base tyre) and the conventional dual-truck tyres. A single wide-base tyre is a proportionately larger and more robust tyre that is now being used on trucks for heavy cargo. This type of tyre is expected to replace dual-tyres in the future, on condition of minimal damage to the existing road infrastructure. To be able to carry the same load as the dual-tyres, the wide-base tyre may have a much greater tyre inflation pressure and a larger individual "footprint" (but could also be smaller than the two combined "footprints" from standard dual-tyres). Research done by De Beer (2008) on tyre-pavement contact stresses has also shown tyre-pavement contact stresses to be, although dependent on the loading magnitude and inflation pressure, mostly rectangular and occasionally circular in shape. Development of solutions for circular surface loading has already been presented in the companion paper published in this edition (Maina *et al* 2017).

In order to develop closed-form solutions for resilient responses of a pavement structure under the rectangular tyre loading, the Cartesian coordinate system may be convenient to use. Bufler (1971) derived the theoretical solution for multi-layered systems using the Cartesian coordinate system for isotropic materials, but did not provide any worked examples. Similarly, Ernian (1989) used both the cylindrical and Cartesian coordinate systems to derive solutions for both circular and rectangular uniformly distributed loads acting on the surface of a multi-layered system with isotropic material properties.

Maina JW, Kawana F, Matsui K. Numerical modelling of flexible pavement incorporating cross-anisotropic material properties – Part II: Surface rectangular loading.
J. S. Afr. Inst. Civ. Eng. 2017:59(1), Art. #1385, 7 pages. http://dx.doi.org/10.17159/2309-8775/2017/v59n1a4

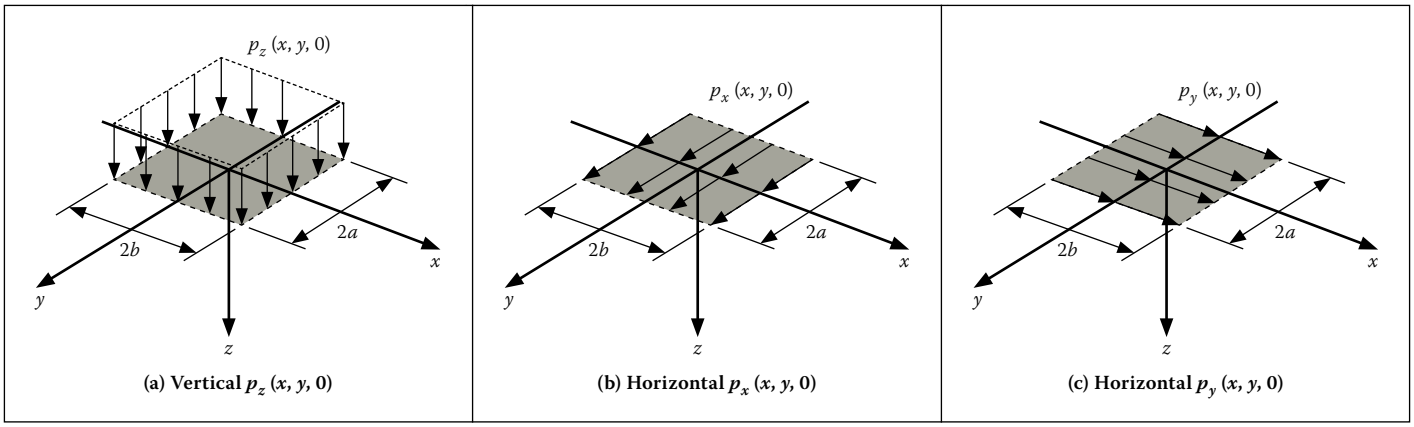

Figure 1 Uniformly distributed rectangular loads

This paper presents the development of closed-form solutions for a multi-layered pavement system under static rectangular loadings, considering both isotropic and cross-anisotropic material properties. Isotropic materials have the same elastic properties in both the vertical and horizontal directions, and can be described by three independent elastic constants – elastic modulus E, Poisson's ratio ν and shear modulus G. In contrast, cross-anisotropy of an elastic material is defined by five independent elastic constants – two elastic moduli in vertical and horizontal directions (E_v, E_h), two Poisson's ratios in vertical and horizontal directions (ν_{vh}, υ_{hh}) and one shear modulus (G_{hv}), as presented by Love (1944).

In this research study, two classical mathematical methods, i.e. classical trigonometric integral and classical potential function, were investigated for flexibility and efficiency. The former was adopted in this study and its use in the determination of pavement responses is presented in this paper. This work is an extension of work where solutions of responses due to circular loading were presented (Maina *et al* 2017). This method is flexible enough and can easily be extended to dynamic and wave propagation problems, although this is not the focus of the paper.

Accuracy and validity of the solutions are verified through comparisons of the computed responses to results obtained using a proprietary finite element package for a five-layer pavement structure, where the four upper main layers were sub-layered, resulting in a pavement system with 17 layers. The pavement layers were composed of materials with isotropic and cross-anisotropic (also known as transversely isotropic) properties.

THEORETICAL DEVELOPMENT

Three-dimensional linear elasticity

For 3D problems shown in Figure 1, the differential equilibrium equations in Cartesian coordinates may be expressed using modified Navier's equations. However, the equations are cumbersome to deal with because of the need to solve three coupled partial differential equations for the three displacement components. The difficulty with finding particular solutions of the system of equations in terms of the displacements arises because each of the sought-after deflection functions in the Cartesian coordinates (x, y and z) appear in all three equilibrium equations.

The solutions may be simplified by representing displacements in terms of harmonic potentials. It is because this approach decouples the equations in various different ways. The most common approach is to use the so-called Papkovich-Neuber potentials to represent the solution (Ozawa *et al* 2009; Borodachev & Astanin 2008). This approach enables the use of a well-known catalogue of particular solutions of the Laplace equation, and sometimes even reduces the problem, if not completely, to one of the classical problems of the theory of harmonic functions (theory of potential). Despite the simplification, it is difficult to extend this approach to problems of dynamic or moving load analysis (Ozawa *et al* 2010).

This paper aims at presenting closed-form solutions of pavement responses due to static rectangular loading in the vertical direction. The solutions presented in this paper were derived based on a more flexible and efficient classical transform integral method. A similar approach can be followed to derive solutions for rectangular loads acting in the longitudinal and transverse directions.

Theoretical development

Three different approaches may be used to solve problems of the theory of elasticity (Borodachev 1995; 2001). In the first approach, the displacement vector is determined first, and this vector is then used to determine the stress and strain tensors (*known as problem in displacements*).

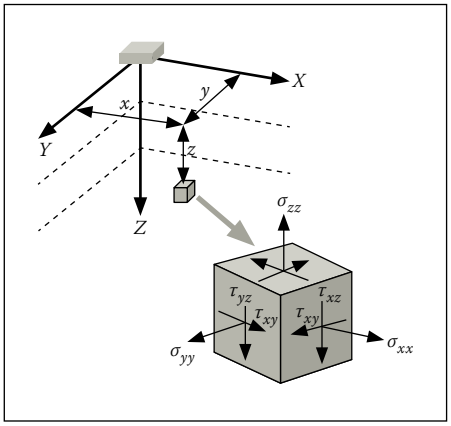

Figure 2 Stress distributions in a Cartesian coordinate system

In the second approach the stress tensor is determined first, and then this tensor is used to determine the strain tensor and displacement vector (*known as problem in stresses*). In the third approach the strain tensor is determined first, and then stress and displacement tensors are determined (*known as problem in strains*). The work presented in this paper followed the first approach, namely *problem in displacements.*

A system of rectangular Cartesian coordinates (x, y, z) is used. By assuming the body forces to be zero, equilibrium equations for an infinitesimal element (Figure 2) can be expressed using Navier's equations as follows (Filonenko-Borodich 1963):

$$\frac{\partial \sigma_x}{\partial x} + \frac{\partial \tau_{xy}}{\partial y} + \frac{\partial \tau_{xz}}{\partial z} = 0 \quad (1)$$

$$\frac{\partial \tau_{xy}}{\partial x} + \frac{\partial \sigma_y}{\partial y} + \frac{\partial \tau_{zy}}{\partial z} = 0 \quad (2)$$

$$\frac{\partial \tau_{xz}}{\partial x} + \frac{\partial \tau_{yz}}{\partial y} + \frac{\partial \sigma_z}{\partial z} = 0 \quad (3)$$

Where: σ_x, σ_y, σ_z are normal stress and τ_{xz}, τ_{yz} and τ_{xy} are shear stresses acting on an infinitesimal element. The two subscripts on the symbols for shear stresses represent, respectively, the face and direction on which the shear stress is acting.

The strain-displacement relationship may be represented as follows:

$$\varepsilon_x = \frac{\partial u}{\partial x}, \varepsilon_y = \frac{\partial v}{\partial y}, \varepsilon_z = \frac{\partial w}{\partial z}, \gamma_{xy} = \frac{\partial v}{\partial x} + \frac{\partial u}{\partial y}, \gamma_{xz} = \frac{\partial u}{\partial z} + \frac{\partial w}{\partial x}, \gamma_{yz} = \frac{\partial w}{\partial y} + \frac{\partial v}{\partial z} \quad (4)$$

Where: $u = u(x, y, z)$, $v = v(x, y, z)$ and $w = w(x, y, z)$ are displacements in the directions of x, y and z axes. Furthermore, ε_x, ε_y and ε_z are normal strains corresponding to normal stresses σ_x, σ_y and σ_z, whereas γ_{xz}, γ_{yz} and γ_{xy} are shear strains corresponding to shear stresses τ_{xz}, τ_{yz} and τ_{xy}.

Generalised Hooke's law

In linear elasticity, if the stress is sufficiently small, Hooke's law is used to represent the material behaviour and to relate the unknown stresses and strains. The general equation for Hooke's law is:

$$\varepsilon_{ij} = s_{ijkl}\,\sigma_{kl} = \sum_{k=1}^{3}\sum_{l=1}^{3} s_{ijkl}\,\sigma_{kl} \quad (5)$$

where $i, j = 1, 2, 3$

In this case s_{ijkl} is a fourth-rank tensor called elastic compliance of the material. Each subscript of s_{ijkl} takes on the values from 1 to 3, giving a total of $3^4 = 81$ independent components in s. However, due to the symmetry of both ε_{ij} and σ_{kl}, the elastic compliance s must satisfy the relation:

$$s_{ijkl} = s_{jikl} = s_{ijlk} = s_{jilk} \quad (6)$$

It follows from Equation 5, therefore, that the generalised Hooke's law in Equation 5 can be simplified to become:

$$\varepsilon_i = s_{ij}\sigma_j, \text{ where } i, j = 1, .., 6 \quad (7)$$

This relationship reduces the number of s components to 36, as seen in the following linear relation between the pseudovector forms of the strain and stress:

$$\begin{Bmatrix}\varepsilon_1\\ \varepsilon_2\\ \varepsilon_3\\ \varepsilon_4\\ \varepsilon_5\\ \varepsilon_6\end{Bmatrix} = \begin{bmatrix}s_{11} & s_{12} & s_{13} & s_{14} & s_{15} & s_{16}\\ s_{21} & s_{22} & s_{23} & s_{24} & s_{25} & s_{26}\\ s_{31} & s_{32} & s_{33} & s_{34} & s_{35} & s_{36}\\ s_{41} & s_{42} & s_{43} & s_{44} & s_{45} & s_{46}\\ s_{51} & s_{52} & s_{53} & s_{54} & s_{55} & s_{56}\\ s_{61} & s_{62} & s_{63} & s_{64} & s_{65} & s_{66}\end{bmatrix} \begin{Bmatrix}\sigma_1\\ \sigma_2\\ \sigma_3\\ \sigma_4\\ \sigma_5\\ \sigma_6\end{Bmatrix} \Rightarrow$$

$$\begin{Bmatrix}\varepsilon_x\\ \varepsilon_y\\ \varepsilon_z\\ \gamma_{yz}\\ \gamma_{xz}\\ \gamma_{xy}\end{Bmatrix} = \begin{bmatrix}s_{11} & s_{12} & s_{13} & s_{14} & s_{15} & s_{16}\\ s_{21} & s_{22} & s_{23} & s_{24} & s_{25} & s_{26}\\ s_{31} & s_{32} & s_{33} & s_{34} & s_{35} & s_{36}\\ s_{41} & s_{42} & s_{43} & s_{44} & s_{45} & s_{46}\\ s_{51} & s_{52} & s_{53} & s_{54} & s_{55} & s_{56}\\ s_{61} & s_{62} & s_{63} & s_{64} & s_{65} & s_{66}\end{bmatrix} \begin{Bmatrix}\sigma_x\\ \sigma_y\\ \sigma_z\\ \tau_{yz}\\ \tau_{xz}\\ \tau_{xy}\end{Bmatrix} \quad (8)$$

The s matrix in this form is also symmetric. It therefore contains only 21 independent elements. The number of independent elements is obtained by counting elements in the upper right triangle of the matrix, including the diagonal elements (i.e. $1 + 2 + 3 + 4 + 5 + 6 = 21$). Furthermore, if the material exhibits symmetry in its elastic response, the number of independent components in the s matrix will be reduced even further.

For example, in the simplest case of isotropic materials whose elastic moduli are the same in all directions, only three unique components (s_{11}, s_{12}, s_{44}) exist, as shown in Equation 9. In the elastic range, these three coefficients of the ordinary isotropic model require three parameters (E, ν, G) for their definitions as follows:

$$s = \begin{bmatrix}s_{11} & s_{12} & s_{12} & 0 & 0 & 0\\ s_{12} & s_{11} & s_{12} & 0 & 0 & 0\\ s_{12} & s_{12} & s_{11} & 0 & 0 & 0\\ 0 & 0 & 0 & s_{44} & 0 & 0\\ 0 & 0 & 0 & 0 & s_{44} & 0\\ 0 & 0 & 0 & 0 & 0 & s_{44}\end{bmatrix} \quad (9)$$

Where: $s_{11} = \frac{1}{E}$, $s_{12} = -\frac{\nu}{E}$, $s_{44} = \frac{1}{G}$, $G = \frac{E}{2(1+\nu)}$

In cross-anisotropic materials, however, six unique components (s_{11}, s_{12}, s_{13}, s_{33}, s_{44}) and s_{66} exist, as shown in Equation 10. These six components of the ordinary cross-anisotropic model require five parameters (E_v, E_h, ν_{hv}, υ_{hh}, G_{hv}) for their definitions (Love 1944).

$$s = \begin{bmatrix}s_{11} & s_{12} & s_{13} & 0 & 0 & 0\\ s_{12} & s_{11} & s_{13} & 0 & 0 & 0\\ s_{13} & s_{13} & s_{33} & 0 & 0 & 0\\ 0 & 0 & 0 & s_{44} & 0 & 0\\ 0 & 0 & 0 & 0 & s_{44} & 0\\ 0 & 0 & 0 & 0 & 0 & s_{66}\end{bmatrix} \quad (10)$$

Where: $s_{11} = \frac{1}{E_h}$, $s_{12} = -\frac{\nu_{hh}}{E_h}$, $s_{13} = -\frac{\nu_{hv}}{E_v}$, $s_{33} = \frac{1}{E_v}$, $s_{44} = \frac{1}{G_{hv}}$, $G_{hv} = \frac{E_v}{2(1+\nu_{hv})}$, $s_{66} = 2(s_{11} - s_{12})$

Writing the stresses in terms of the strains would require Equation 8 to be inverted, yielding:

$$\sigma_i = c_{ij}\,\varepsilon_j \quad (11)$$

Where: c_{ij} is a fourth-rank tensor called elastic stiffness of the material. The stiffness and compliance matrices in Equation 11 are related in the following form:

$$c = s^{-1} \quad (12)$$

Three components (c_{11}, c_{12}, c_{44}) exist for isotropic materials, whereas, in cross-anisotropic materials, five unique components (c_{11}, c_{12}, c_{13}, c_{33}, c_{44}, c_{66}) exist. It should be noted that a special cross-anisotropy solution exists, where $E_v = E_h$ and $\nu_{vh} = \upsilon_{hh}$. Equation 13 shows the six components of the elastic stiffness matrix, whereas Equations 14–19 define each of these six components:

$$c = \begin{bmatrix}c_{11} & c_{12} & c_{13} & 0 & 0 & 0\\ c_{12} & c_{11} & c_{13} & 0 & 0 & 0\\ c_{13} & c_{13} & c_{33} & 0 & 0 & 0\\ 0 & 0 & 0 & c_{44} & 0 & 0\\ 0 & 0 & 0 & 0 & c_{44} & 0\\ 0 & 0 & 0 & 0 & 0 & c_{66}\end{bmatrix} \quad (13)$$

Where:

$$c_{11} = \frac{E_h(-E_v + E_h\nu_{hv}^2)}{(1+\nu_{hh})(-E_v + E_v\nu_{hh} + 2E_h\nu_{hv}^2)} \quad (14)$$

$$c_{12} = -\frac{E_h(E_v\nu_{hh} + E_h\nu_{hv}^2)}{(1+\nu_{hh})(-E_v + E_v\nu_{hh} + 2E_h\nu_{hv}^2)} \quad (15)$$

$$c_{13} = -\frac{E_hE_v\nu_{hv}}{-E_v + E_v\nu_{hh} + 2E_h\nu_{hv}^2} \quad (16)$$

$$c_{33} = \frac{E_v^2(-1+\nu_{hh})}{-E_v + E_v\nu_{hh} + 2E_h\nu_{hv}^2} \quad (17)$$

$$c_{44} = G = \frac{E_v}{2(1+\nu_{hv})} \quad (18)$$

$$c_{66} = \frac{E_v}{2(1+\nu_{hv})} = \frac{(c_{11} - c_{12})}{2} \quad (19)$$

Substituting Equation 13 in 11 yields:

$$\begin{Bmatrix}\sigma_x\\ \sigma_y\\ \sigma_z\\ \tau_{yz}\\ \tau_{xz}\\ \tau_{xy}\end{Bmatrix} = \begin{bmatrix}c_{11} & c_{12} & c_{13} & 0 & 0 & 0\\ c_{12} & c_{11} & c_{13} & 0 & 0 & 0\\ c_{13} & c_{13} & c_{33} & 0 & 0 & 0\\ 0 & 0 & 0 & c_{44} & 0 & 0\\ 0 & 0 & 0 & 0 & c_{44} & 0\\ 0 & 0 & 0 & 0 & 0 & c_{66}\end{bmatrix} \begin{Bmatrix}\varepsilon_x\\ \varepsilon_y\\ \varepsilon_z\\ \gamma_{yz}\\ \gamma_{xz}\\ \gamma_{xy}\end{Bmatrix} \quad (20)$$

Derivation of the solutions

It is convenient to use the three-dimensional Cartesian coordinate system and make an assumption that displacement functions $u(x, y, z)$, $v(x, y, z)$ and $w(x, y, z)$ in the x, y and z directions, respectively, may be represented using double trigonometric functions, as detailed below. With this approach, the x and y dependencies of the displacement functions $u(x, y, z)$, $v(x, y, z)$ and $w(x, y, z)$ are accommodated by means of analytical double integral Fourier transform, with the z dependence approximated by using closed-form solutions.

The Fourier transform of the displacements employs transform pairs that are

defined in terms of the Fourier parameters in the x and y directions (ξ_x and ξ_y) as follows:

$$\tilde{u}(\xi_x, \xi_y, z) = \int_{-\infty}^{\infty}\int_{-\infty}^{\infty} u(z)\sin(\xi_x x)\cos(\xi_y y)d\xi_x\, d\xi_y \quad (21)$$

$$\tilde{v}(\xi_x, \xi_y, z) = \int_{-\infty}^{\infty}\int_{-\infty}^{\infty} v(z)\cos(\xi_x x)\sin(\xi_y y)d\xi_x\, d\xi_y \quad (22)$$

$$\tilde{w}(\xi_x, \xi_y, z) = \int_{-\infty}^{\infty}\int_{-\infty}^{\infty} w(z)\cos(\xi_x x)\cos(\xi_y y)d\xi_x\, d\xi_y \quad (23)$$

Where: $\tilde{u}(\xi_x, \xi_y, z)$, $\tilde{v}(\xi_x, \xi_y, z)$ and $\tilde{w}(\xi_x, \xi_y, z)$ are the Fourier transforms of displacement functions about the coordinate z (Sneddon 1951). The procedure that follows is to expand Equation 20 and to express strains in terms of elastic displacements based on Equation 4. After that the Fourier transforms of the displacements using Equations 21, 22 and 23 are applied. Then the resulting functions are substituted into Equations 1–3 to yield their Fourier transforms as follows:

$$-\left(\tilde{u}(\xi_x, \xi_y, z)(\xi_y^2(c_{11}-c_{12}) + 2c_{11}\xi_x^2) + \xi_x\xi_y(c_{11}+c_{12})\,\tilde{v}(\xi_x, \xi_y, z) + 2\xi_x(c_{13}+c_{44})\frac{\partial\tilde{w}(\xi_x, \xi_y, z)}{\partial z} - 2c_{44}\frac{\partial^2\tilde{u}(\xi_x, \xi_y, z)}{\partial z^2}\right) = 0 \quad (24)$$

$$-\left(\xi_x, \xi_y(c_{11}+c_{12})\tilde{u}(\xi_x, \xi_y, z) + \tilde{v}(\xi_x, \xi_y, z)(\xi_x^2(c_{11}-c_{12})\,2c_{11}\xi_y^2) + 2\xi_y(c_{13}+c_{44})\frac{\partial\tilde{w}(\xi_x, \xi_y, z)}{\partial z} - 2c_{44}\frac{\partial^2\tilde{v}(\xi_x, \xi_y, z)}{\partial z^2}\right) = 0 \quad (25)$$

$$\left((c_{13}+c_{44})\left(\xi_x\frac{\partial\tilde{u}(\xi_x, \xi_y, z)}{\partial z} + \xi_y\frac{\partial\tilde{v}(\xi_x, \xi_y, z)}{\partial z}\right) + c_{33}\frac{\partial^2\tilde{w}(\xi_x, \xi_y, z)}{\partial z^2} - c_{44}\tilde{w}(\xi_x, \xi_y, z)(\xi_x^2+\xi_y^2)\right) = 0 \quad (26)$$

Equations 24–26 can be simplified further by representing a differential function with respect to z as $\lambda\left(=\frac{\partial}{\partial z}\right)$ as well as making the following substitutions:

$$a = \frac{c_{11}-c_{12}}{2c_{44}},\ b = \frac{c_{11}+c_{12}}{2c_{44}},\ c = \frac{c_{13}+c_{44}}{c_{44}},\ d = \frac{c_{44}}{c_{33}},\ f = \frac{c_{13}+c_{44}}{c_{33}} \quad (27)$$

and

$$\xi = \sqrt{\xi_x^2+\xi_y^2} \quad (28)$$

Using Equations 27 and 28 it becomes convenient to eliminate $\tilde{u}(\xi_x, \xi_y, z)$ and $\tilde{v}(\xi_x, \xi_y, z)$ from Equations 24–26, then simplify to obtain:

$$(\lambda^4 - t_1\xi^2\lambda^2 + t_2\xi^4)\tilde{w} = 0 \quad (29)$$

The roots of Equation 29 are determined as:

$$\lambda = \pm\xi\sqrt{\frac{t_1 \pm \sqrt{t_1^2-4t_2}}{2}} \quad (30)$$

Where: $t_1 = (b + (a+d) - cf)$, $t_2 = a\,d + b\,d$ from Equation 27.

Putting back the differential function in Equation 29 yields:

$$\left(\frac{\partial^4}{\partial z^4} - t_1\xi^2\frac{\partial^2}{\partial z^2} + t_2\xi^4\right)\tilde{w} = 0 \quad (31)$$

With reference to the roots in Equation 30, the solution form of Equation 31 depends on the sign of the coefficient $t_1^2 - 4t_2$.

Furthermore, and this is very important, depending on the numerical integration methods used, it may be necessary to modify the solution for $\tilde{w}$ to obtain stable and accurate responses of the pavement structure. The solutions presented hereunder were based on the numerical methods used in this research.

1. Solution 1: $t_1^2 - 4t_2 > 0$, where $E_h > E_v$

$$\tilde{w} = \tilde{w}(\xi_x, \xi_y, z) = C_1(\xi)e^{\lambda_1 z} + C_2(\xi)e^{-\lambda_1 z} + C_3(\xi)e^{\lambda_2 z} + C_4(\xi)e^{-\lambda_2 z} \quad (32)$$

Where:

$$\lambda_1 = \xi\sqrt{\frac{t_1+\sqrt{t_1^2-4t_2}}{2}},\ \lambda_2 = \xi\sqrt{\frac{t_1-\sqrt{t_1^2-4t_2}}{2}},$$

and $C_1(\xi)$, $C_2(\xi)$, $C_3(\xi)$, and $C_4(\xi)$ are coefficients of integration determined, as described later, by using boundary loading conditions.

In order to obtain stable and accurate results of pavement responses, Equation 32 was modified to:

$$\tilde{w}(\xi_x, \xi_y, z) = C_1(\xi)\cosh(r_2 z)\,e^{r_1 z} + C_2(\xi)\cosh(r_2 z)\,e^{-r_1 z} - C_3(\xi)\sinh(r_2 z)\,e^{r_1 z} - C_4(\xi)\sinh(r_2 z)\,e^{-r_1 z} \quad (33)$$

Where:

$$r_1 = \xi\left(\frac{\sqrt{t_1-\sqrt{t_1^2-4t_2}} + \sqrt{t_1+\sqrt{t_1^2-4t_2}}}{2\sqrt{2}}\right), \text{ and}$$

$$r_2 = \xi\left(\frac{\sqrt{t_1+\sqrt{t_1^2-4t_2}} - \sqrt{t_1-\sqrt{t_1^2-4t_2}}}{2\sqrt{2}}\right)$$

2. Solution 2: $t_1^2 - 4t_2 = 0$, where $E_h = E_v$

$$\tilde{w}(\xi_x, \xi_y, z) = e^{\xi z}\left(-C_1(\xi)\frac{\xi_y}{\xi} - C_3(\xi)\frac{\xi}{\xi_x} + C_5(\xi)\left(\frac{3c_{11}-c_{12}}{\xi_x(c_{11}+c_{12})} - \frac{z\xi}{\xi_x}\right)\right) + e^{-\xi z}\left(C_2(\xi)\frac{\xi_y}{\xi} + C_4(\xi)\frac{\xi}{\xi_x} + C_6(\xi)\left(\frac{3c_{11}-c_{12}}{\xi_x(c_{11}+c_{12})} + \frac{z\xi}{\xi_x}\right)\right) \quad (34)$$

3. Solution 3: $t_1^2 - 4t_2 < 0$, where $E_h < E_v$

$$\tilde{w}(\xi_x, \xi_y, z) = C_1(\xi)e^{\lambda_1 z} + C_2(\xi)e^{-\lambda_1 z} + C_3(\xi)e^{\lambda_2 z} + C_4(\xi)e^{-\lambda_2 z} \quad (35)$$

Where:

$$\lambda_1 = \xi\frac{\sqrt{t_1+\sqrt{t_1^2-4t_2}}}{2}, \text{ and}$$

$$\lambda_2 = \xi\frac{\sqrt{t_1-\sqrt{t_1^2-4t_2}}}{2}$$

For stable and accurate results of pavement responses, Equation 35 was modified to:

$$\tilde{w}(\xi_x, \xi_y, z) = C_1(\xi)\cos(r_2 z)\,e^{r_1 z} + C_2(\xi)\cos(r_2 z)\,e^{-r_1 z} - C_3(\xi)\sin(r_2 z)\,e^{r_1 z} - C_4(\xi)\sin(r_2 z)\,e^{-r_1 z} \quad (36)$$

Where:

$$r_1 = \left(\xi\sqrt{\frac{t_1}{2}}\right) \text{ and } r_2 = \left(\xi\sqrt{\frac{t_1^2-4t_2}{2}}\right)$$

Solutions for the remaining Fourier transformed displacements

Substituting Equations 33, 34 and 36 into Equations 24 and 25, the solutions for $\tilde{u}(\xi_x, \xi_y, z)$ and $\tilde{v}(\xi_x, \xi_y, z)$ are derived.

As an example, solutions for $\tilde{u}(\xi_x, \xi_y, z)$ and $\tilde{v}(\xi_x, \xi_y, z)$ for the case where $E_h = E_v$ (***solution 2***) are obtained as follows:

$$\tilde{u}(\xi_x, \xi_y, z) = C_2(\xi)e^{\xi z} + C_4(\xi)e^{-\xi z} + C_5(\xi)ze^{\xi z} + C_6(\xi)ze^{-\xi z} \quad (37)$$

$$\tilde{v}(\xi_x, \xi_y, z) = e^{\xi z}\left(C_1(\xi) + C_3(\xi)\frac{\xi_y}{\xi_x} + C_5(\xi)\frac{\xi_y}{\xi_x}z\right) + e^{-\xi z}\left(C_2(\xi) + C_4(\xi)\frac{\xi_y}{\xi_x} + C_6(\xi)\frac{\xi_y}{\xi_x}z\right) \quad (38)$$

Solutions for $\tilde{u}(\xi_x, \xi_y, z)$, $\tilde{v}(\xi_x, \xi_y, z)$ and $\tilde{w}(\xi_x, \xi_y, z)$ are then substituted into Equations 4 and 20 to determine the Fourier transforms of normal and shear

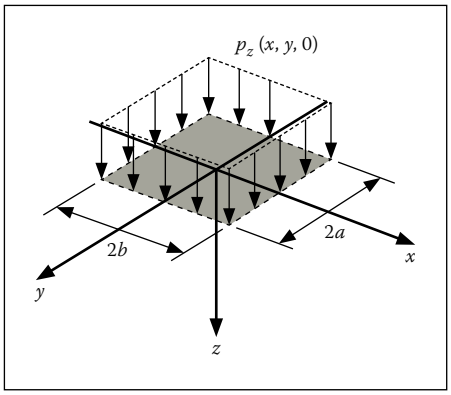

Figure 3 Surface rectangular vertical load ($p_z(x, y, z) = 0$)

stresses $\tilde{\sigma}_x(\xi_x, \xi_y, z)$, $\tilde{\sigma}_y(\xi_x, \xi_y, z)$, $\tilde{\sigma}_z(\xi_x, \xi_y, z)$, $\tilde{\tau}_{xz}(\xi_x, \xi_y, z)$, $\tilde{\tau}_{yz}(\xi_x, \xi_y, z)$, and $\tilde{\tau}_{xy}(\xi_x, \xi_y, z)$.

Boundary condition – surface rectangular vertical loading

For the loading case shown in Figure 3, there is only a single uniformly distributed surface rectangular vertical load, P, whose sides are $2 \times a$ and $2 \times b$ in dimensions. Boundary conditions for rectangular loads acting on a surface of a semi-infinite medium shown in in Figure 3 may be represented by taking into consideration the equilibrium between external and internal vertical and shear stresses, as shown below:

When $x \leq |a|$ and $y \leq |b|$ then:

$$\begin{Bmatrix} \tilde{\sigma}_z^1(\xi_x, \xi_y, z=0) \\ \tilde{\tau}_{xz}^1(\xi_x, \xi_y, z=0) \\ \tilde{\tau}_{yz}^1(\xi_x, \xi_y, z=0) \end{Bmatrix} = - \begin{Bmatrix} \tilde{p}_z(\xi_x, \xi_y, z=0) \\ 0 \\ 0 \end{Bmatrix} \quad (39)$$

Where:

$$\tilde{p}_z(\xi_x, \xi_y) = \int_{-a}^{a} \int_{-b}^{b} - \frac{p_z \cos(\xi_x x) \cos(\xi_y y)}{2\pi} d(\xi_y) d(\xi_x) = - \frac{2p_z \sin(\xi_x x) \sin(\xi_y y)}{\xi_x \xi_y \pi} \text{ and}$$

$$p_z = \frac{P}{(2 \times a)(2 \times b)}$$

In addition, when $x > |a|$ and $y > |b|$ then:

$$\begin{Bmatrix} \tilde{\sigma}_z^1(\xi_x, \xi_y, z=0) \\ \tilde{\tau}_{xz}^1(\xi_x, \xi_y, z=0) \\ \tilde{\tau}_{yz}^1(\xi_x, \xi_y, z=0) \end{Bmatrix} = \begin{Bmatrix} 0 \\ 0 \\ 0 \end{Bmatrix} \quad (40)$$

Pavement responses

By applying Fourier inverse transformation of all the Fourier transformed solutions, it is possible to determine solutions for pavement responses at any point in a pavement structure.

$$u(x, y, z) = \frac{1}{2\pi} \int_{-\infty}^{\infty} \int_{-\infty}^{\infty} \tilde{u}(k_x, k_y, z) \sin(\xi_x x) \cos(\xi_y y) d\xi_x d\xi_y \quad (41)$$

$$v(x, y, z) = \frac{1}{2\pi} \int_{-\infty}^{\infty} \int_{-\infty}^{\infty} \tilde{v}(\xi_x, \xi_y, z) \cos(\xi_x x) \sin(\xi_y y) d\xi_x d\xi_y \quad (42)$$

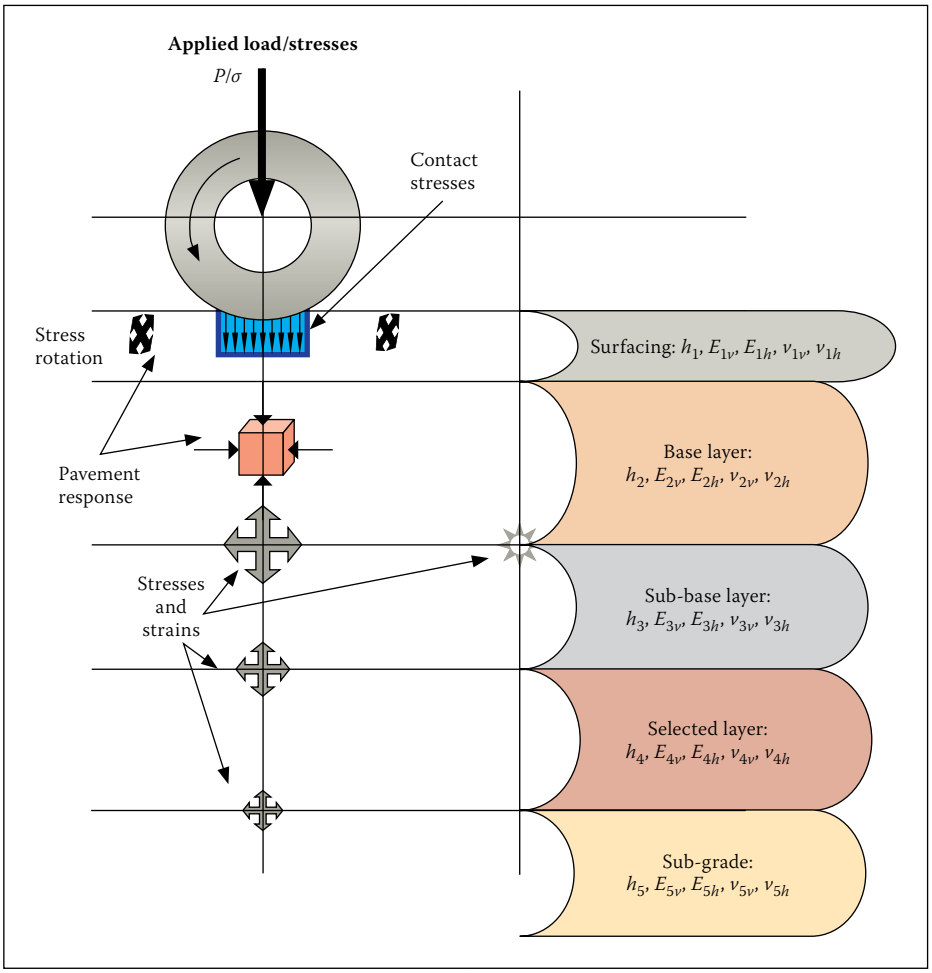

Figure 4 Hypothetical pavement structure

Table 1 Profile of the hypothetical pavement structure

Layer type	Layer number	E-Modulus vert (MPa)	E-Modulus horiz (MPa)	P-Ratio vert	P-Ratio horiz	Thickness (mm)	Slip rate
AC	1	20 281	18 618	0.14	0.13	10	0
AC	2	19 781	19 767	0.15	0.15	10	0
AC	3	19 303	19 282	0.15	0.15	10	0
AC	4	18 846	15 583	0.12	0.11	10	0
G1	5	450	450	0.35	0.35	37.5	0
G1	6	450	450	0.35	0.35	37.5	0
G1	7	450	450	0.35	0.35	37.5	0
G1	8	450	450	0.35	0.35	37.5	0
C3	9	250	250	0.35	0.35	75	0
C3	10	250	250	0.35	0.35	75	0
C3	11	250	250	0.35	0.35	75	0
C3	12	250	250	0.35	0.35	75	0
G7	13	50	50	0.45	0.45	37.5	0
G7	14	50	50	0.45	0.45	37.5	0
G7	15	50	50	0.45	0.45	37.5	0
G7	16	50	50	0.45	0.45	37.5	0
SG	17	239	239	0.4	0.4	Semi-infinite	

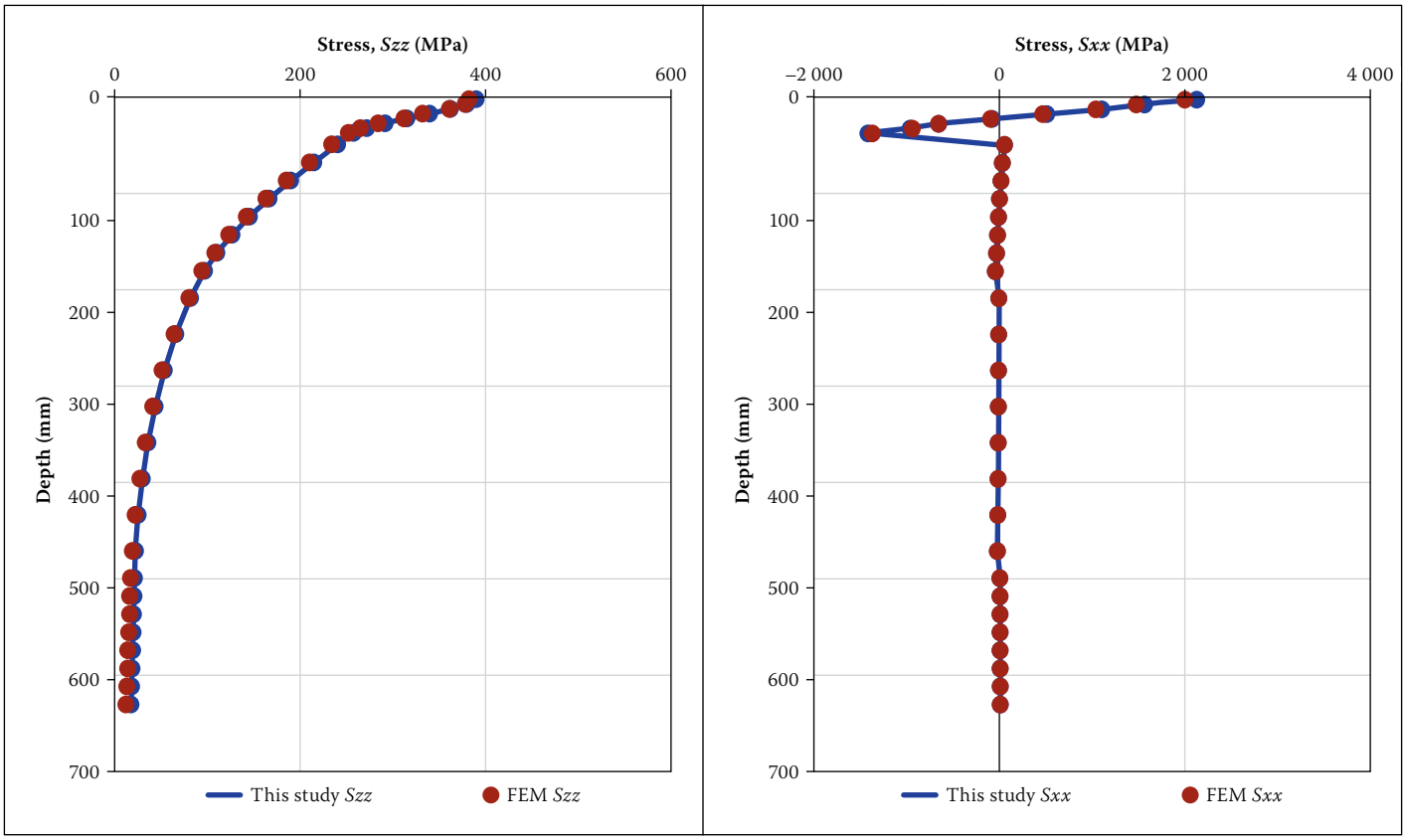

Figure 5 Stress distribution under the centre of the load with depth between this study and proprietary FEM package

$$w(x, y, z) = \frac{1}{2\pi}\int_{-\infty}^{\infty}\int_{-\infty}^{\infty}\bar{w}(\xi_x, \xi_y, z)\cos(\xi_x x)\sin(\xi_y y)d\xi_x d\xi_y \quad (43)$$

$$\sigma_x(x, y, z) = \frac{1}{2\pi}\int_{-\infty}^{\infty}\int_{-\infty}^{\infty}\bar{\sigma}_x(\xi_x, \xi_y, z)\cos(\xi_x x)\cos(\xi_y y)d\xi_x d\xi_y \quad (44)$$

$$\sigma_y(x, y, z) = \frac{1}{2\pi}\int_{-\infty}^{\infty}\int_{-\infty}^{\infty}\bar{\sigma}_y(\xi_x, \xi_y, z)\cos(\xi_x x)\cos(\xi_y y)d\xi_x d\xi_y \quad (45)$$

$$\sigma_z(x, y, z) = \frac{1}{2\pi}\int_{-\infty}^{\infty}\int_{-\infty}^{\infty}\bar{\sigma}_z(\xi_x, \xi_y, z)\cos(\xi_x x)\cos(\xi_y y)d\xi_x d\xi_y \quad (46)$$

$$\tau_{xz}(x, y, z) = \frac{1}{2\pi}\int_{-\infty}^{\infty}\int_{-\infty}^{\infty}\bar{\tau}_{xz}(\xi_x, \xi_y, z)\sin(\xi_x x)\cos(\xi_y y)d\xi_x d\xi_y \quad (47)$$

$$\tau_{yz}(x, y, z) = \frac{1}{2\pi}\int_{-\infty}^{\infty}\int_{-\infty}^{\infty}\bar{\tau}_{yz}(\xi_x, \xi_y, z)\cos(\xi_x x)\sin(\xi_y y)d\xi_x d\xi_y \quad (48)$$

$$\tau_{xy}(x, y, z) = \frac{1}{2\pi}\int_{-\infty}^{\infty}\int_{-\infty}^{\infty}\bar{\tau}_{xy}(\xi_x, \xi_y, z)\sin(\xi_x x)\sin(\xi_y y)d\xi_x d\xi_y \quad (49)$$

WORKED EXAMPLES

Solutions developed in this study were used to compute responses at different positions within a pavement structure. The pavement structure for which the simulation results are presented here is shown in Figure 4. Based on historical tyre loading on South African roads, a tyre vertical load of 21.5 kN on a rectangular patch of 231 mm by 238 mm resulting in a 390 kPa contact stress was used in the analysis (De Beer 2008). All layers, except the asphalt layer, were modelled with isotropic, linear-elastic properties. The asphalt layer was modelled with cross-anisotropic, linear elastic properties. Information on all the layers, including sub-layers, is shown in Table 1. The sub-layering of the upper four main layers into four layers each resulted in a total of 17 layers, as shown in Table 1.

The vertical stiffness in the asphalt sub-layers shows a marginal increase close to the surface that may be attributed to binder ageing, but more probably to a slight reduction in the temperature conditions. The top and bottom asphalt sub-layers show significant reduction in the effective horizontal stiffness resulting from cracking initiating from both the top and bottom of the main asphalt layer.

Discussion of results

Figures 5 and 6 show comparisons between the numerical method developed in this study and a proprietary FEM package for stresses (*Szz*) and (*Sxx*) as well as strains (*Ezz*) and (*Exx*) distributions with depth, *z*-direction, under the centre of a rectangular surface load of magnitude 21.5 kN (390 kPa contact stress). From these results it is clear that the closed-form solutions developed in this study have achieved a very good level of accuracy, as their results compare well with results from a proprietary FEM package.

It is also important to mention here that the software developed from this work has become the analysis engine for the new SAPDM (South African Pavement Design Method).

What is also evident in the strains plots is that, as the FEM increases the size of the elements at points far from where the load is acting, the accuracy is reduced a little bit and the results start moving away from the results of this study. However, all in all, the agreement of the two methods, i.e. approximation by FEM and closed-form solution developed in this paper, is very good.

CONCLUSIONS

1. A numerical tool for analysis of an elastic multilayer system under the action of a surface rectangular load, considering both cross-anisotropic and isotropic material properties, has successfully been developed.
2. The numerical tool developed in this study is capable of performing analyses for an unlimited number of points in an elastic multi-layered pavement system with an unlimited number of layers, and on the surface where an unlimited number of uniformly distributed rectangular loads act.

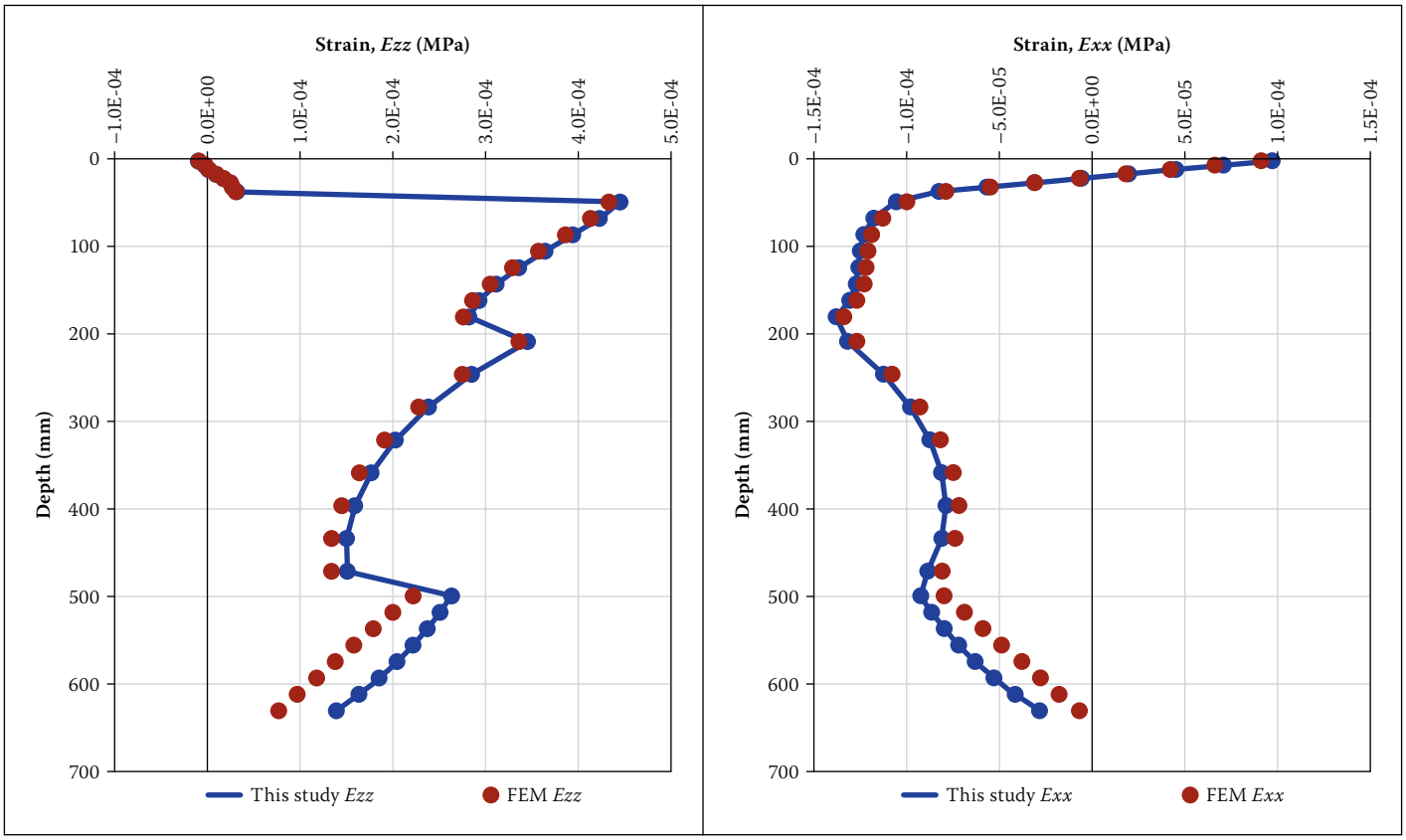

Figure 6 Strain distribution under the centre of the load with depth between this study (closed-form) and proprietary FEM package

3. The results shown in this paper confirm the accuracy and reliability of the closed-form theoretical solutions developed.
4. A very good match of the stress results was obtained between the numerical tool developed in this study and a proprietary FEM package.
5. Differences in the strain results at points far from where the load acts, were observed. The differences seem to be emanating from the FEM, which is a proprietary package. In conventional FEM, stress computations come after strain computations, and the trends should have been similar. The reason for the differences is not clear, but the results, as measured, are nevertheless reported here.
6. The numerical tools developed can be used to improve the design, evaluation and analysis of multi-layered road/runway pavement systems.

ACKNOWLEDGEMENTS

This research study was part of the revision of the SAPDM, a project sponsored by the South African National Roads Agency SOC Ltd (SANRAL) and the Council for Scientific and Industrial Research (CSIR). The incentive funding for rated researchers received from the National Research Foundation (NRF) is also gratefully acknowledged, as well as the support from Dr Hechter Theyse for setting up the numerical problem together with Prof Rudi Du Preez to run the proprietary FEM analyses for comparative purposes.

REFERENCES

Borodachev, N M 1995. Three-dimensional problem of the theory of elasticity in strains. *Strength of Materials*, 27(5–6): 296.

Borodachev, N M 2001. Construction of exact solutions to three-dimensional elastic problems in stresses. *International Applied Mechanics*, 39(6): 438.

Borodachev, N M & Astanin, V V 2008. Solution of a three-dimensional problem of the elasticity theory in terms of displacements for an isotropic elastic layer. *Strength of Materials*, 40(3): 308–315.

Bufler, H 1971. Theory of elasticity of a multilayered medium. *Journal of Elasticity*, 1(2): 125–143.

De Beer, M 2008. Stress-In-Motion (SIM) – A new tool for road infrastructure protection? *Proceedings*, International Conference on Heavy Vehicles, WIM Session 7, 19–22 May, Paris/Marne-la-Vallée.

Ernian, P 1989. Static response of a transversely isotropic and layered half-space to general surface loads. *Physics of the Earth and Planetary Interiors*, 54: 353–363.

Filonenko-Borodich, M 1963. *Theory of Elasticity*. Moscow: Peace Publishers.

Love, A 1944. *A Treatise on the Mathematical Theory of Elasticity*. New York: Dover Publications.

Maina, J W, Kawana F & Matsui, K 2017. Numerical modelling of flexible pavement incorporating cross-anisotropic material properties – Part I: Surface circular loading. *Journal of South African Institution of Civil Engineering*, 59(1): 22–27.

Ozawa, Y, Maina, J W & Matsui, K 2009. Linear elastic analysis of pavement structure loaded over rectangular area. Paper presented at the 88th Transportation Research Board Annual Meeting, 11–15 January, Washington, DC. (CD-ROM.)

Ozawa, Y, Maina, J W & Matsui, K 2010. Analysis of multilayered half space due to rectangular moving load. Paper presented at the 89th Transportation Research Board Annual Meeting, 10–14 January, Washington, DC. (CD-ROM.)

Sneddon, I N 1951. *Fourier Transforms*. New York: McGraw-Hill.